



**HAL**  
open science

## Live-cell imaging and mathematical analysis of the “community effect” in apoptosis

Diane Coursier, David Coulette, H el ene Leman, Emmanuel Grenier, Gabriel  
Ichim

► **To cite this version:**

Diane Coursier, David Coulette, H el ene Leman, Emmanuel Grenier, Gabriel Ichim. Live-cell imaging and mathematical analysis of the “community effect” in apoptosis. 2022. hal-03821641

**HAL Id: hal-03821641**

**<https://hal.science/hal-03821641>**

Preprint submitted on 28 Oct 2022

**HAL** is a multi-disciplinary open access archive for the deposit and dissemination of scientific research documents, whether they are published or not. The documents may come from teaching and research institutions in France or abroad, or from public or private research centers.

L’archive ouverte pluridisciplinaire **HAL**, est destin ee au d ep ot et  a la diffusion de documents scientifiques de niveau recherche, publi es ou non,  emanant des  tablissements d’enseignement et de recherche fran ais ou  trangers, des laboratoires publics ou priv es.



Distributed under a Creative Commons Attribution 4.0 International License



## 31 **Abstract**

32 As a cellular intrinsic mechanism leading to cellular demise, apoptosis  
33 was thoroughly characterized from a mechanistic perspective. Nowadays  
34 there is an increasing interest in describing the non-cell autonomous or  
35 community effects of apoptosis, especially in the context of resistance to  
36 cancer treatments. Transitioning from cell-centered to cell population-relevant  
37 mechanisms adds a layer of complexity for imaging and analyzing an  
38 enormous number of apoptotic events. In addition, the community effect  
39 between apoptotic and living cells is difficult to be taken into account for  
40 complex analysis. We describe here a robust and easy to implement method  
41 to analyze the interactions between cancer cells, while under apoptotic  
42 pressure. Using this approach we showed as proof-of-concept that apoptosis  
43 is insensitive to cellular density, while the proximity to apoptotic cells  
44 increases the probability of a given cell to undergo apoptosis.

## 45 **Introduction**

46 Inconspicuous at the single cell level, apoptosis is a powerful  
47 mechanism when triggered at the organismal level. It is the sculpting force  
48 behind all multicellular organism morphogenesis, ensuring all organs have the  
49 right size, supernumerary cells are removed and neurons innervate the  
50 correct targets.

51 In cancer, apoptosis is an efficient guardian against oncogenic  
52 transformation and it is the preferred mechanism employed by tumor  
53 suppressor proteins to eliminate dangerous rogue cells (1). For instance, p53  
54 can trigger apoptosis by up-regulating the expression of several pro-apoptotic  
55 proteins (1). Apoptosis is undeniably the main executioner of most cancer  
56 drugs and radiotherapy (2).

57 Apoptosis is triggered when one of two distinct pathways is engaged:  
58 the extrinsic or the intrinsic. Extrinsic apoptosis relies on the stimulation of a  
59 death receptor-family member (e.g., TRAIL-R, FAS or TNF-R) by a TNF-  
60 related cytokine, and activation of caspase 8 and 10 via the death-inducing  
61 signaling complex (DISC) (3). The intrinsic pathway is initiated by an  
62 intracellular death stimulus such as DNA damage, chemo- and radiotherapy

63 or tumor suppressor activation. In this case, the point of no return is  
64 mitochondrial outer-membrane permeabilization (or MOMP) followed by  
65 cytochrome *c* release, apoptosome assembly and activation of caspase 9 and  
66 then 3 and 7. Mitochondrial permeabilization is tightly regulated by the BCL-2  
67 family proteins that can be anti-apoptotic (BCL-2, BCL-xL or MCL-1), pro-  
68 apoptotic (BID, BIM, BAD, PUMA or NOXA) and effector pore-forming  
69 proteins such as BAX or BAK (for review see (4)).

70         Once apoptosis is triggered, this does not inevitably lead to cell death,  
71 as it is now accepted that cells can survive if mitochondrial permeabilization  
72 does not affect all mitochondria or if the ESCRT-III complex restores plasma  
73 membrane integrity (5) (6) (7). Currently, there is a lack of understanding of  
74 how and why the kinetics of apoptosis varies so much between cells or  
75 following different treatments.

76         The heterogeneous response to apoptosis is also described in isogenic  
77 cancer cell lines. This is puzzling since these cells are genetically identical  
78 and should express similar levels of both pro- and anti-apoptotic proteins.  
79 Cellular heterogeneity to undergo apoptosis thus appears to originate from  
80 non-genetic transcriptional variability. This translates into cell-to-cell variations  
81 of pro- and anti-apoptotic protein expression and activity. For instance, the  
82 Lahav group elegantly showed that there is a high variability of p53 response  
83 to DNA damaging agents; apoptotic cells accumulate p53 much faster and  
84 earlier, while this accumulation is delayed in resistant cells, allowing time for  
85 the up-regulation of pro-survival IAP (inhibitor of apoptosis) proteins (8).

86         Recent publications shed light on the effects apoptotic cells exert on  
87 neighboring cells. They can actively release EGFR ligands, FGF2 or Wnt3 to  
88 boost the survival and proliferation of neighboring cells (9) (10) (11). This  
89 paracrine crosstalk is also complemented by mechanotransduction  
90 mechanisms triggered by tissue stretching around apoptotic cells, which  
91 involves the Yes-associated protein (YAP) pathway (12).

92         There is therefore an increasing need to accurately estimate the  
93 variability of apoptosis induction in a given cell population. To achieve this, we  
94 developed a medium-throughput imaging pipeline using apoptotic cell  
95 markers, coupled with mathematical analysis. This allowed us to unveil a  
96 neighboring effect for apoptosis induction, irrespective of cell death stimuli or

97 cell density, whereby the probability of undergoing apoptosis increases in the  
98 proximity of apoptotic cells. Hence, the combined application of imaging and  
99 computational analysis to evaluate the response to a given apoptotic stimulus  
100 may provide new insight into misunderstood phenomena such as fractional  
101 killing or apoptosis-induced proliferation, which are major concerns in the  
102 context of apoptosis-based cancer therapies.

## 103 **Results**

### 104 *Live-cell imaging system to trigger and measure multi-stimuli apoptosis*

105 To mathematically analyze the kinetics of apoptotic cell death while  
106 varying different parameters, we first set up a cellular system allowing  
107 medium-throughput quantification of apoptosis at the cell population level. For  
108 this, we used melanoma WM115 cells stably expressing mCherry-tagged  
109 histone H2B (H2B-mCherry) to spatially identify the exact topology of a given  
110 cell (**Figure 1A**). Following treatment with an apoptotic stimulus, the induction  
111 of apoptosis is easily visualized using the live cell-impermeant dye SYTOX  
112 Green (SG). Live cells can thus be identified by the nuclear-localized H2B-  
113 mCherry-only signal (red nuclei), whereas apoptotic cells appear yellow,  
114 owing to the colocalization of H2B-mCherry and green SG (**Figure 1A**). Next,  
115 we used various stimuli to trigger apoptosis. Treatment with TNF $\alpha$  and  
116 cycloheximide (CHX) was initially used as a model for death receptor-  
117 mediated apoptosis. Of note, CHX enhances TNF $\alpha$ -induced apoptosis by  
118 blocking the translation of short-lived anti-apoptotic proteins (13). Downstream  
119 of the TNF $\alpha$  receptor 1/2 (TNFR1/2), the DISC activates caspase 8 and  
120 triggers MOMP via BID cleavage (**Figure 1B**). To induce intrinsic apoptosis,  
121 we used two death stimuli: first, a combination of BH3 mimetics ABT-737  
122 inactivating the anti-apoptotic proteins BCL2, BCL-xL and BCL-w, and UMI-77  
123 targeting MCL1; second, a doxycycline (dox)-inducible WM115 cell line to  
124 activate the mitochondrial pore-forming protein BAX (**Figure 1B**). These  
125 apoptotic stimuli were then applied to SG-pre-loaded WM115 H2B-mCherry  
126 cells plated at different densities and imaged periodically (1 or 2 hours  
127 intervals) using the IncuCyte live-cell imager (**Figure 1A**).

128           Next, we validated the induction of apoptosis by assessing the  
129 processing of effector caspase-3 into p17/p19 fragments and the cleavage of  
130 PARP1, which is a hallmark of apoptosis effectiveness. As shown In **Figure**  
131 **2A** and **B**, treatment with TNF $\alpha$ /CHX (TC), BH3 mimetics (BH3m) and  
132 increasing doses of doxycycline efficiently induced apoptosis. Of note,  
133 caspase-3 processing and PARP1 cleavage were blocked by treatment with  
134 the pan-caspase inhibitor Q-VD-OPh. In addition, IncuCyte-based live-cell  
135 imaging was used to delineate the kinetics of apoptosis triggered by the  
136 different stimuli described above (**Figure 2C, D**). Apoptotic cells were marked  
137 by SG and quantified over time, with image acquisitions every 1-2 hours over  
138 a period of 48 hours on average. **Figure 2E** shows this imaging method can  
139 efficiently detect and discriminate between living cells (mCherry-positive) and  
140 apoptotic cells (SG-positive). The figure presents results of TNF $\alpha$ /CHX and  
141 BH3 mimetics treatment, albeit the same was observed for WM115 cells  
142 overexpressing BAX (data not shown).

143           Using this cell model of apoptosis induction, coupled with medium-  
144 throughput live-cell imaging we therefore established an imaging technique  
145 able to monitor the heterogeneous induction of apoptosis at the cell  
146 population level.

147

#### 148 ***Cell clustering has no effect on the incidence of apoptosis***

149           Following different pro-apoptotic treatments (**Figure 1B**) and IncuCyte-  
150 based live cell imaging, we obtained datasets of H2B-mCherry images (red  
151 images) and the corresponding SYTOX Green staining (green images) at  
152 different time points, for a kinetics analysis of 48 hours. We then designed two  
153 independent pipelines to segment H2B-mCherry-marked nuclei, one based on  
154 the CellProfiler software and the other written in Python, using standard image  
155 libraries to ensure a robust analysis (**Figure 1A**). The analysis pipeline  
156 included the following steps. First, for a pair of red/green images the output is  
157 a segmented “red” image with a known red object centroid position ( $X_i$ ,  $Y_i$ )  
158 onto which a measurement of the green signal is superposed ( $I_i$ , representing  
159 the maxima green signal intensity) (**Figure 3A**). Second, for a given time-point  
160  $t$ , the analysis pipeline retrieves a set of  $N$  red centroid positions ( $X_i$ ,  $Y_i$ ) with  
161 their associated SYTOX Green intensity signal  $I_i$ . Data analysis is then

162 performed using three parameters  $\delta$ ,  $n$  and  $I_t$ , where  $\delta$  is the inter-cellular  
163 distance at which another cell(s) is/are considered to be in contact and could  
164 influence each other,  $n$  is the threshold number of neighboring cells above  
165 which a cell is considered to be in a cluster and  $I_t$  is the threshold intensity of  
166 SYTOX Green, derived from background noise, above which the cell is  
167 considered to be apoptotic. Of note, two cells are considered neighbors if the  
168 distance between their centroids is below  $\delta$  (**Figure 3A**).

169 Once we determined  $\delta$ ,  $n$  and  $I_t$ , we determined for each cell whether it  
170 was apoptotic (A) or not ( $\bar{A}$ ). We then established the relationships of  
171 proximity between cells (the so-called neighboring effect) by determining for  
172 each cell whether it was in a cluster of cells regardless of their apoptotic  
173 status (C) or with a known apoptotic status (Ca) (**Figure 3B**). This method is  
174 well suited to quantify spatial relations between apoptotic cells.

175 Using this approach, we were first interested in determining whether a  
176 correlation between cell clustering and apoptosis (between C and A). This is  
177 driven by previous work suggesting that cell density is an important modulator  
178 of both extrinsic and intrinsic apoptosis (14) (15-17).

179 By examining three scenarios, in which a given cell was considered to  
180 be in a cluster if it was surrounded by 1, 2 or 3 neighboring cells (regardless  
181 of their apoptotic status), we found that a cell with no neighbors ( $\bar{C}$ ) had the  
182 same probability of entering apoptosis as a cell in a cluster (of 1, 2, or 3  
183 neighboring cells) (**Figure 3C-E** for TNF $\alpha$ /CHX treatment). We then computed  
184 and plotted the time dependent  $p$ -value of a Fisher exact test that evaluates  
185 the independence between A and C (**Figure 3C-E**, bottom panels). Of note, if  
186 the  $p$ -value is high (as in **Figure 3C-E**, bottom panels), this means that the  
187 hypothesis that A and C are independent cannot be rejected. In other words,  
188 this means that the probability of being apoptotic whenever one cell has  
189 neighboring relation(s) (probability  $p(A/C)$ , blue curve in **Fig. 3C-E**, top  
190 panels) and the probability of being apoptotic when one cell is isolated  
191 (probability  $p(A/\bar{C})$ , orange curve) might be equal.

192 The same holds true when triggering intrinsic apoptosis with BH3  
193 mimetics (**Figure 3F**) or when overexpressing the pro-apoptotic protein BAX  
194 (**Figure 3G**). Though these results were obtained at low cell density, we

195 confirmed their relevance for cells grown at a high density (**Supplementary**  
196 **Figure 1**).

197 Hence, these data suggest that cell clustering has no impact on the  
198 occurrence of apoptosis.

199

### 200 *The induction of apoptosis is enhanced by the proximity of a cell to an* 201 *apoptotic cell*

202 Next, we tested whether the proximity of a cell with one apoptotic cell  
203 or an apoptotic cluster (up to three apoptotic neighboring cells) was correlated  
204 with its propensity to undergo apoptosis. We obtained results in complete  
205 contrast to Figure 3, as the probability to enter apoptosis when in proximity  
206 with one or more apoptotic cells (probability  $p(A/C_a)$ , blue curve) was  
207 significantly higher than the probability to enter apoptosis when isolated from  
208 apoptotic cells (probability  $p(A/C_a)$ , orange curve) (**Figure 4A-C** for  
209 TNF $\alpha$ /CHX treatment). Indeed, the  $p$ -value (Fisher's exact test) was  
210 significantly low ( $p < 0.05$ ) for the intermediate time points, meaning that both  
211 probabilities cannot be considered as equal. We observed a higher  $p$ -value at  
212 the beginning and the end of the kinetics, which does not affect our analysis,  
213 since there are few apoptotic cells at beginning of the time-course and, at the  
214 end, most cells are apoptotic and the neighboring effect saturates. This  
215 observation also holds true for treatment with BH3 mimetics and BAX  
216 overexpression (**Figure 4 D, E**). Finally, we validated these data at a higher  
217 cellular density (**Supplementary Figure 2**).

218 Taken together, our analysis pipeline reveals that apoptosis induction  
219 is influenced by a neighboring effect: the likelihood of a cell to undergo  
220 apoptosis is significantly higher when it is in proximity with apoptotic cells.

## 221 **Discussion**

222 Defective induction of cell death is the cause on many diseases,  
223 ranging from cancer to neurodegenerative diseases, and it is therefore  
224 important to study its propagative nature using appropriate tools.

225 Here, we report the development of an analysis pipeline for medium-  
226 throughput imaging of apoptotic cancer cells that integrates several key



227 parameters: temporal dimension, topographic localization of both living (cells  
228 stably expressing the mCherry-tagged histone 2B) and apoptotic (SYTOX  
229 Green-positive) cells, while applying several apoptotic stimuli.

230 Using this approach, we found that cancer cells have a similar  
231 probability of undergoing apoptosis if they are in proximity or not with other  
232 cells of unknown status. In other words, cell crowding does not have a  
233 protective effect against apoptosis. However, a cell is more likely to become  
234 apoptotic if it is in close contact with apoptotic neighboring cells. This holds  
235 true for all of the apoptotic stimuli we tested, either extrinsic or intrinsic  
236 inducers of apoptosis. These results are in line with Bhola and Simon's study  
237 demonstrating that daughter cells, with a high likelihood of being in proximity,  
238 synchronously undergo apoptosis. This synchrony is lost as cells become less  
239 related over time (18). Apoptotic synchrony is therefore transiently heritable  
240 and is lost due to noise in protein translation (19). To take into account  
241 progeny and monitor cell proliferation history, we would need to introduce into  
242 our imaging pipeline a lineage tracer such as the one developed by Oren and  
243 colleagues (20).

244 Our experimental settings are in 2D cellular cultures, yet one might  
245 apply it to 3D cultures such as cancer organoids. For this, however, the  
246 sample will require transparization and 3D imaging microscopy. Here, the  
247 proof-of-concept is provided for apoptosis, though the protocol could easily be  
248 adapted to other types of programmed cell death, such as caspase-  
249 independent cell death, necroptosis or pyroptosis. Importantly, this method  
250 could also be helpful in identifying factors facilitating or inhibiting cell death  
251 propagation. Similar methods were developed to quantify the occurrence of  
252 fractional killing, a barrier for effective cancer treatments, and helped establish  
253 mediators such as the anti-apoptotic protein MCL1 (21) (22).

254 Recent research clearly demonstrates that while apoptosis is  
255 immunologically silent, it still involves releasing a plethora of signaling  
256 molecules that impinge on the fate of surrounding cells. The term of  
257 apoptosis-induced apoptosis was coined in *Drosophila*, where apoptotic cells  
258 in the wing disk triggered apoptosis in trans by secreting Eiger (the TNF  
259 homologue in flies), and stimulating pro-apoptotic JNK signaling (23). The  
260 same holds true in mammals during the regressive phase of the hair follicle

261 (23). In cancer, the radiation-induced bystander effect, through which  
262 irradiated cells lead to the death of non-irradiated neighboring cells, is also a  
263 good example of this concept (24). Interestingly, recent studies revealed the  
264 rapid propagation of ferroptotic cell death, and the analysis pipeline described  
265 herein might provide further mechanistic insights (25) (26). Inversely,  
266 apoptosis-induced proliferation has been unveiled and describes a state in  
267 which dying cells release prostaglandins and Wnt3, instructing the  
268 proliferation of nearby cells (27) (11). Recently, the group of Tait showed that  
269 apoptotic cells also release FGF2 to enhance the anti-apoptotic resilience in  
270 trans (10).

271 The analysis method developed here could increase and enrich our  
272 knowledge on “community effects” of cell death so that they can be blocked or  
273 enhanced, according to the physio-pathological context.

## 274 **Material and methods**

### 275 *Cell lines*

276 Human melanoma cells WM115 (a gift from R. Insall – The Beatson Institute,  
277 Glasgow, UK) were maintained in DMEM supplemented with 2 mM L-  
278 glutamine (ThermoFisher Scientific, 25030-24), non-essential amino acids  
279 (ThermoFisher Scientific, 11140-035), 1 mM sodium pyruvate (ThermoFisher  
280 Scientific, 11360-039), 10% FBS (Eurobio, CVFSVF00-01) and 1%  
281 penicillin/streptomycin (ThermoFisher Scientific, 15140-122).

282

### 283 *Stable cell line generation*

284 For retroviral transduction, Phoenix Ampho 293T cells ( $2 \times 10^6$  in 10 cm in  
285 diameter Petri dishes) were transfected with pQXIN H2B-mCherry (gift from  
286 Dr. Luca Fava) using Lipofectamine 2000 (ThermoFisher Scientific,  
287 11668019). Twenty-four hours later, the virus-containing supernatant was  
288 filtered and used to infect WM115 cells in the presence of 1  $\mu\text{g}/\text{mL}$  polybrene  
289 (Sigma-Aldrich, H9268). This was repeated with fresh viral supernatant 48  
290 hours later. Melanoma cells stably expressing H2B-mCherry were further  
291 purified by cell sorting. WM115 H2B mCherry cells with doxycycline-inducible  
292 expression of the BAX protein were created using the Sleeping Beauty

293 transposon system (28). The plasmids used were piTR1 BAX (gift from David  
294 Goldschneider) and pCMV(CAT)T7-SB100 (Addgene, 34879) for the  
295 expression of SB100X transposase. WM115 H2B mCherry cells were then co-  
296 transfect with piTR1 BAX and pCMV(CAT)T7-SB100 plasmids using  
297 Lipofectamine 2000 and selected with puromycin (1 µg/mL).

298

### 299 *Western blotting*

300 Cell lysates were prepared using NP-40 lysis buffer (1% NP-40, 1 mM EDTA,  
301 150 mM NaCl, 50 mM Tris pH 7.4, 1 mM PMSF, Complete Protease Inhibitors  
302 (Sigma-Aldrich, 4693116001)). Protein content was determined by Bio-Rad  
303 assay, then 25-50 µg of proteins were separated on SDS-polyacrylamide gels  
304 (Biorad) under denaturing conditions (SDS PAGE sample loading buffer  
305 (VWR, GENO786-701) supplemented with 1 mM DTT) and finally transferred  
306 onto nitrocellulose. Membranes were probed with the following antibodies at a  
307 1/1,000 dilution unless otherwise stated: BAX (2772, Cell Signaling),  
308 Caspase-3 (9662, Cell Signaling), PARP1 (9542, Cell Signaling), β-tubulin  
309 (2146, Cell Signaling).

310 The nitrocellulose membranes were rinsed 3 times for 10 min in TBS-Tween  
311 0.1% and then incubated with appropriate secondary antibody coupled to  
312 HRP for 1 hour at room temperature. Finally, the proteins of interest were  
313 detected using Clarity Western ECL (Biorad, 1705060) and chemiDoc imager  
314 (Biorad, 17001401).

315

### 316 *IncuCyte imager-based cell viability assay*

317 Cell viability was determined using an IncuCyte Zoom imaging system  
318 (Sartorius). Cells were seeded onto Imagelock 96-well plates in media  
319 containing 30 nM SYTOX Green (Life Technologies, S7020). Following  
320 different apoptotic treatments, the cells were imaged every 60 or 120 minutes  
321 and the analysis of the SYTOX Green-positive cells was performed using the  
322 available IncuCyte image analysis software (Essen Bioscience).

323

### 324 *Modeling the progression of apoptosis*

### 325 ***Data description***

326 Nuclei, set as objects, are delineated at each time step using automatic  
327 segmentation of mCherry fluorescence ("Red") images via the CellProfiler  
328 pipeline for primary objects, which is tuned to detect blob-like structures. The  
329 "apoptosis" signal is obtained by measuring the maximum intensity over each  
330 nucleus object of the "Green" fluorescence image. A threshold value for this  
331 intensity  $I_t$  is chosen, which defines the fluorescence intensity considered as  
332 sufficient for a given nucleus to be considered as apoptotic. In the results  
333 presented herein, the threshold chosen was 0.2 that corresponds to 2/3 to 1/2  
334 of the maximum intensity of the Green signal.

### 335 ***Statistical test***

336 For a given time frame, segmentation data consist in a sequence of nuclei  
337 positions  $(X_i, Y_i)$  and green signal intensity  $I_i$ , with  $i$  varying from 1 to  $N$ , where  
338  $N$  is the total number of nuclei objects for this time frame.

### 339 ***Apoptotic variable A***

340 Given the intensity threshold  $I_t$ , we defined the class A of apoptotic cells as  
341 the set of nuclei such that  $I_i \geq I_t$ .

### 342 ***Clustering (density) C and apoptotic clustering $C_a$ variables***

343 In order to separate "clustered" cells from isolated ones, we set a  
344 characteristic interaction distance  $\delta$  and a threshold  $n$  on the number of  
345 neighbors. An object at position  $(X_i, Y_i)$  is considered to be part of a cluster  
346 (*i.e.*, in the class C) if there are a least  $n$  nuclei inside the disk of radius  $\delta$  and  
347 center  $(X_i, Y_i)$ . An object at position  $(X_i, Y_i)$  is considered to be part of an  
348 apoptotic cluster (*i.e.*, in the class  $C_a$ ) if there are a least  $n$  apoptotic nuclei  
349 (*i.e.*, in the class A) inside the disk of radius  $\delta$  and center  $(X_i, Y_i)$ .

### 350 ***Independence tests***

351 We used classical Fisher's exact test to determine if random variables A and  
352 C are independent and subsequently if random variables A and  $C_a$  are  
353 independent. In this setting, for the simplicity of notation, we identify the class  
354 A with the random variable that indicates if an object belongs or not to the  
355 class A, and similarly for classes C and  $C_a$ . We gave exact  $p$ -values for this  
356 test. Generally, the null hypothesis (the considered pair of random variables

357 are independent of each other) can be rejected when the  $p$ -value is lower than  
358 0.05.

359

## 360 **Acknowledgements**

361 Funding from Institute Convergence PLAsCAN (ANR-17-CONV-0002), LabEx  
362 DEVweCAN (University of Lyon), Agence Nationale de la Recherche (ANR)  
363 Young Researchers Project (ANR-18-CE13-0005-01), La Ligue Nationale  
364 Contre le Cancer and Fondation de France supported this work. We thank  
365 Brigitte Manship for reviewing the manuscript.

## 366 **Author contributions**

367 Conceptualization, G. Ichim, D. Coulette, H.L. and E.G.; Methodology, G.  
368 Ichim, D. Coulette, H.L. and E.G.; Formal analysis, G. Ichim, D. Coulette and  
369 H.L.; Investigation, G. Ichim, D.C., D. Coulette and H.L.; Resources, G. Ichim,  
370 D. Coulette, H.L. and E.G.; Writing – Original Draft and Editing, G. Ichim; All  
371 authors reviewed and edited the manuscript; Supervision, G. Ichim, D.  
372 Coulette, H.L. and E.G.; Project administration and funding acquisition, G.  
373 Ichim.

## 374 **Figure legends**

375 **Figure 1. Imaging and quantification of apoptosis induction using live**  
376 **and dead cell markers.**

377 **A.** Overview of the live/dead cell imaging and computer analysis protocol.

378 **B.** Apoptotic signaling induced by treatment with TNF $\alpha$ /CHX or BH3 mimetics,  
379 or through BAX overexpression (aCasp8 - active Caspase-8; aCasp 3/7 –  
380 active Caspase-3 and -7, tBID – truncated BID).

381

382 **Figure 2. Validation of the apoptosis induction protocols.**

383 **A.** WM115 H2B-mCherry cells were treated either with TNF $\alpha$ /CHX (TC) (50  
384 ng/mL of TNF $\alpha$  and 5  $\mu$ g/mL CHX) or BH3 mimetics ABT-737/UMI-77 (10  $\mu$ M  
385 each) for 12 hours in the presence or absence of the pan-caspase inhibitor Q-

386 VD-OPh (10  $\mu$ M). Protein lysates were then probed for the expression and  
387 processing of PARP1 and Caspase-3. Tubulin was used as a loading control.

388 **B.** WM115 H2B-mCherry cells were treated with 1 or 2.5  $\mu$ g/mL of doxycycline  
389 (dox) to induce BAX expression for 12 hours in the presence or absence of Q-  
390 VD-OPh (10  $\mu$ M) and then analyzed as described in (A).

391 **C-D.** IncuCyte imager-based quantification of apoptotic WM115 H2B mCherry  
392 cells (SYTOX Green-positive cells) following treatment with TNF $\alpha$ /CHX (TC),  
393 ABT-737/UMI-77 (**C**) or doxycycline (at 1 or 2.5  $\mu$ g/mL) (**D**).

394 **E.** Representative images of phase-contrast, H2B-mCherry and SYTOX  
395 Green signal from WM115 H2B-mCherry cells treated as described in (A).

396

397 **Figure 3. Apoptosis occurs independently of cell clustering.**

398 **A-B.** Definition of the parameters taken into account for the mathematical  
399 analysis of the effect cell clustering has on apoptosis induction. Cells with the  
400 nucleus half in red half in green are either alive or apoptotic, respectively.

401 **C-E.** Probability estimates (upper panels) and the corresponding *p-value*  
402 (lower panels) for the occurrence of apoptosis in TNF $\alpha$ /CHX-treated WM115  
403 H2B-mCherry cells surrounded by 1, 2 or 3 neighboring cells.

404 **F-G.** Similar analysis as in (C-E), for WM115 H2B-mCherry cells treated with  
405 ABT-737/UMI-77 (**F**) and doxycycline (**G**). The neighboring effect for 1 cell is  
406 shown.

407

408 **Figure 4. Apoptotic cell clusters influence the life-death decisions in**  
409 **neighboring cells.**

410 **A-C.** Probability estimates (upper panels) and the corresponding *p-value*  
411 (lower panels) for the occurrence of apoptosis in TNF $\alpha$ /CHX-treated WM115  
412 H2B-mCherry cells surrounded by 1, 2 or 3 apoptotic neighboring cells.

413 **D-E.** Similar analysis as in (A-C), for WM115 H2B-mCherry cells treated with  
414 ABT-737/UMI-77 (**D**) and doxycycline (**E**). The neighboring effect for 1  
415 apoptotic cell is shown.

416

417 **Supplementary Figure 1 (related to Figure 3).**

418 **A, B.** Probability estimates (upper panels) and the corresponding  $p$ -value  
 419 (lower panels) for the occurrence of apoptosis in ABT-737/UMI-77-treated  
 420 WM115 H2B-mCherry cells surrounded by 2 or 3 neighboring cells.

421 **C, D.** Similar analysis as in (A, B), albeit apoptosis was triggered by  
 422 doxycycline induction of pro-apoptotic BAX protein.

423

424 **Supplementary Figure 2 (related to Figure 4).**

425 **A, B.** Probability estimates (upper panels) and the corresponding  $p$ -value  
 426 (lower panels) for the occurrence of apoptosis in ABT-737/UMI-77-treated  
 427 WM115 H2B-mCherry cells surrounded by 2 or 3 apoptotic neighboring cells.

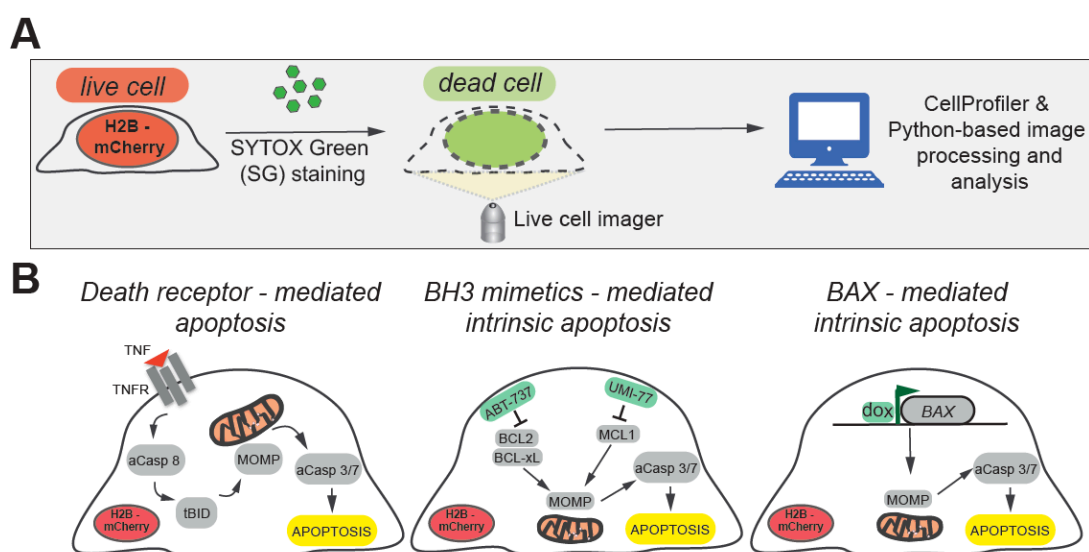
428 **C, D.** Similar analysis as in (A, B), albeit apoptosis was triggered by  
 429 doxycycline induction of pro-apoptotic BAX protein.

430

431

432

## Figure 1



433

434

435

436

437

438

439

440

441

442

443

## Figure 2

444

445

446

447

448

449

450

451

452

453

454

455

456

457

458

459

460

461

462

463

464

465

466

467

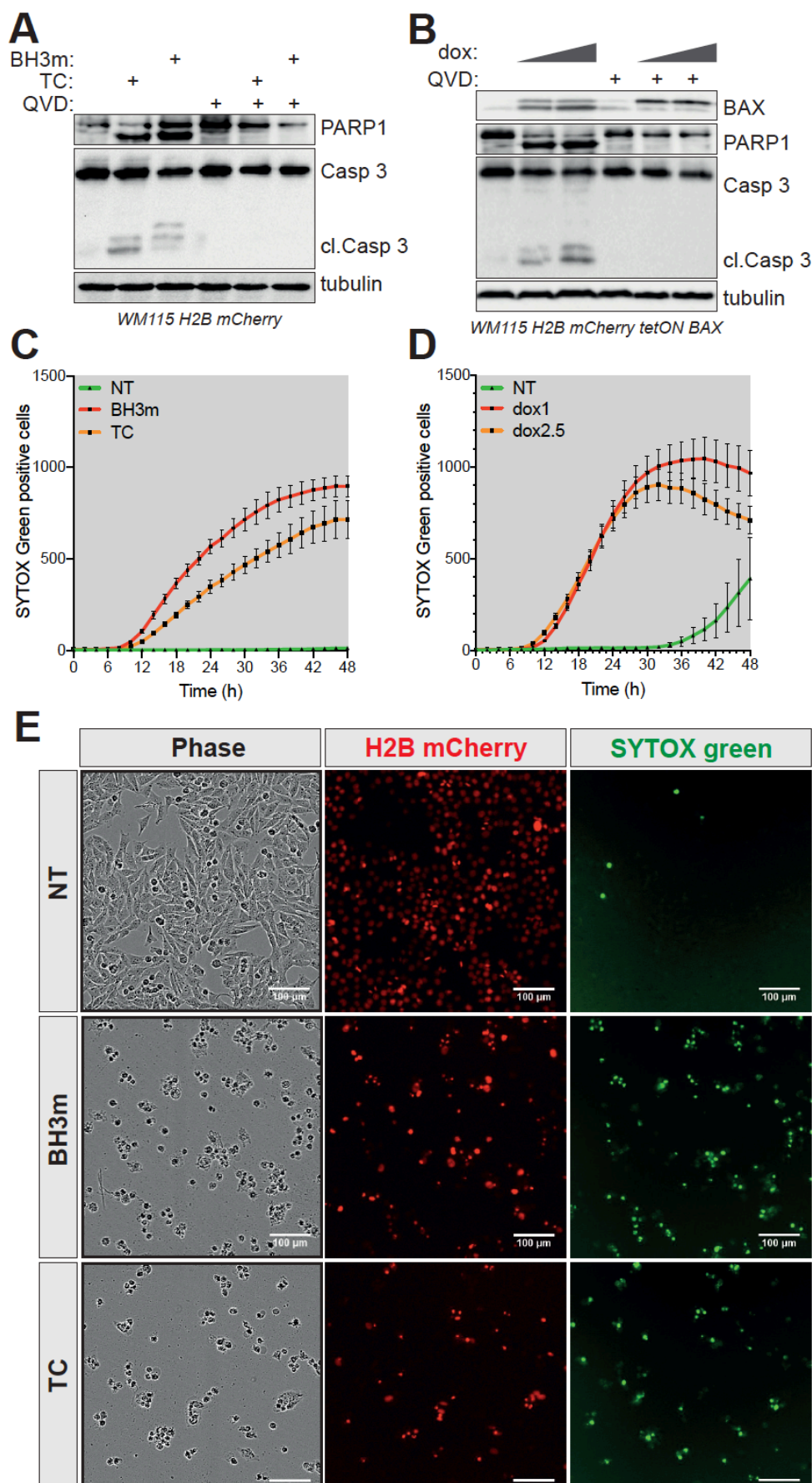
468

469

470

471

472





473

474

475

476

477

478

479

480

481

482

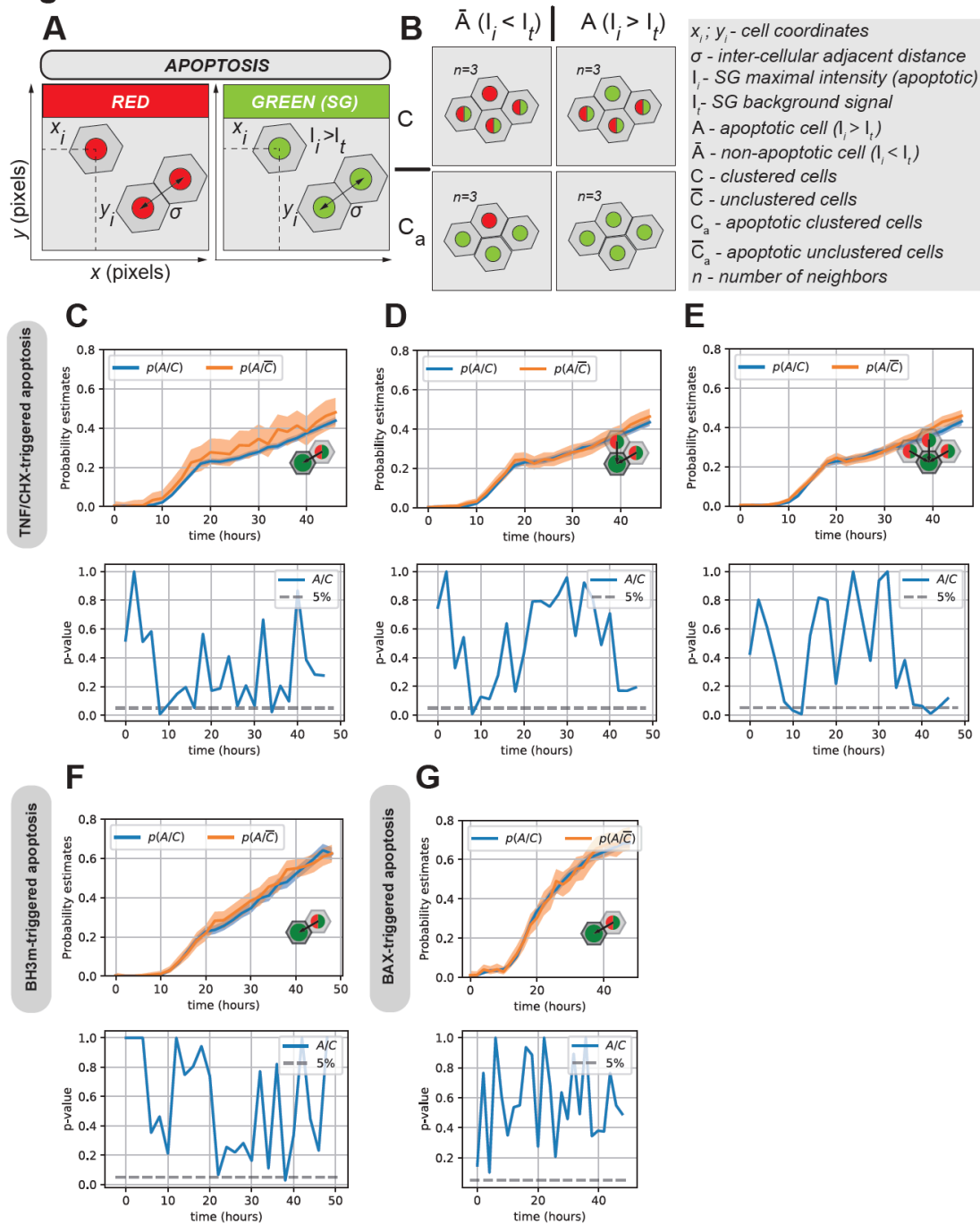
483

484

485

486

**Figure 3**



487

488

489

490

491

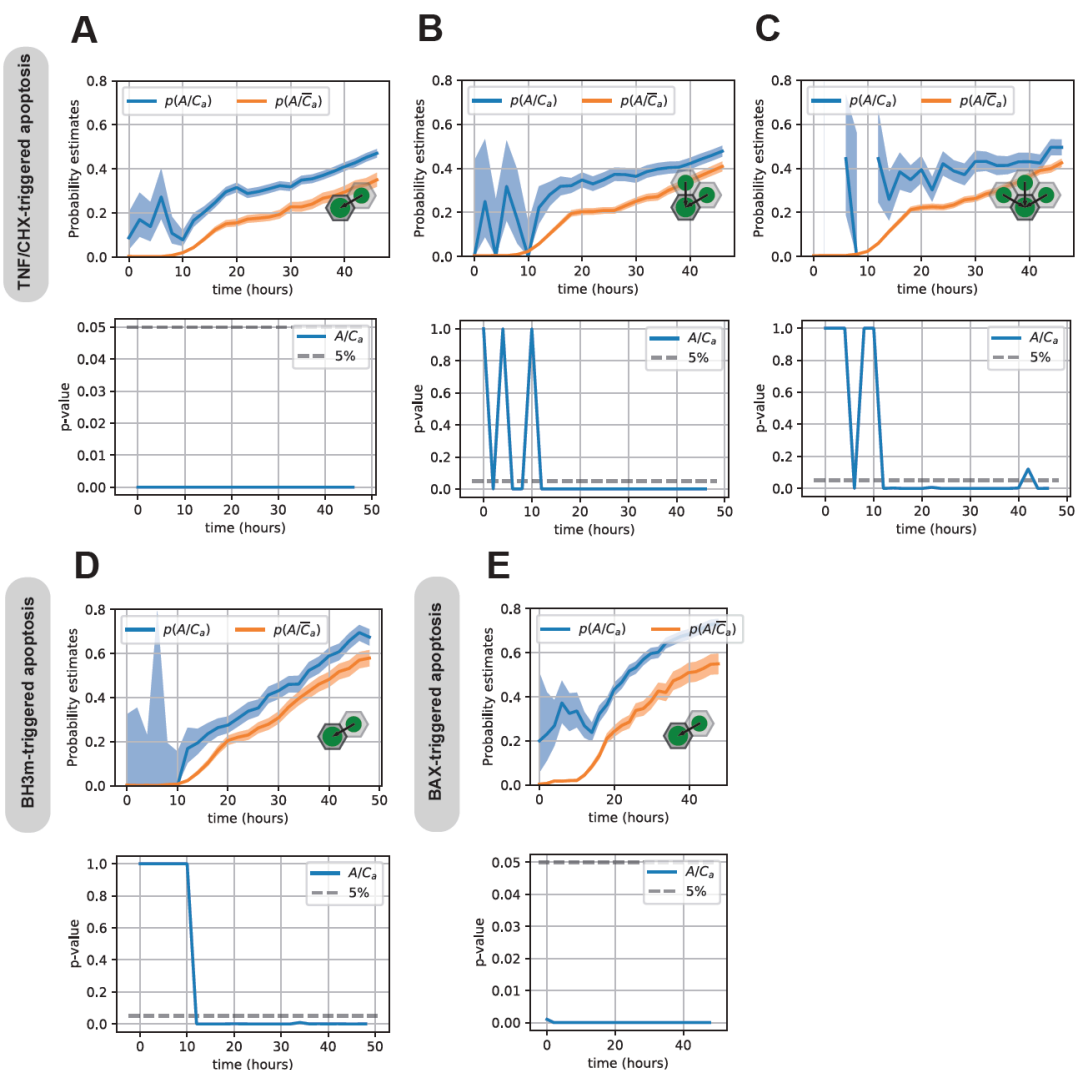
492

493

494

495

**Figure 4**



496

497

498

499

500

501

502

503

504

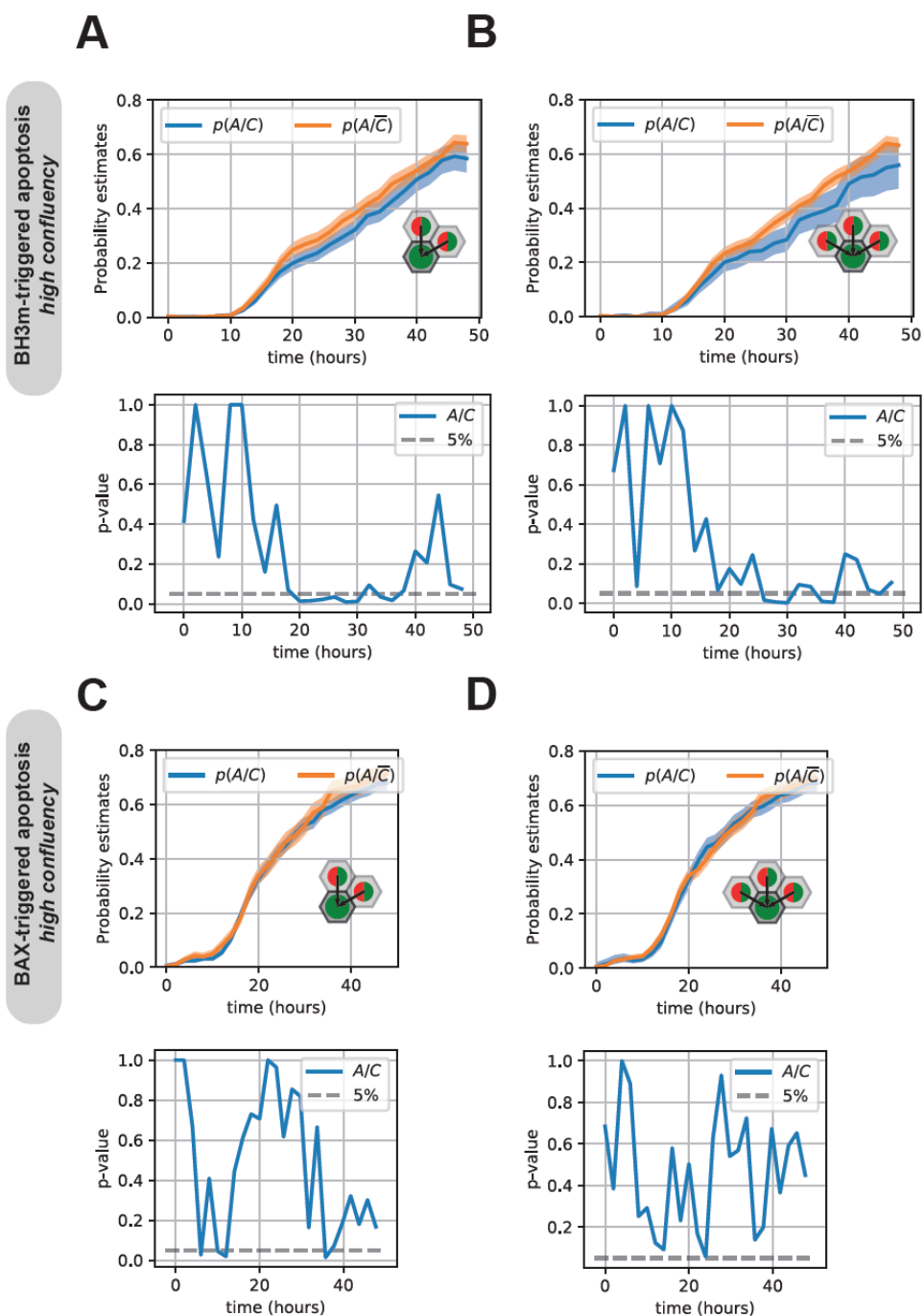
505

506

507

508

## Supplementary Figure 1



555

536

537

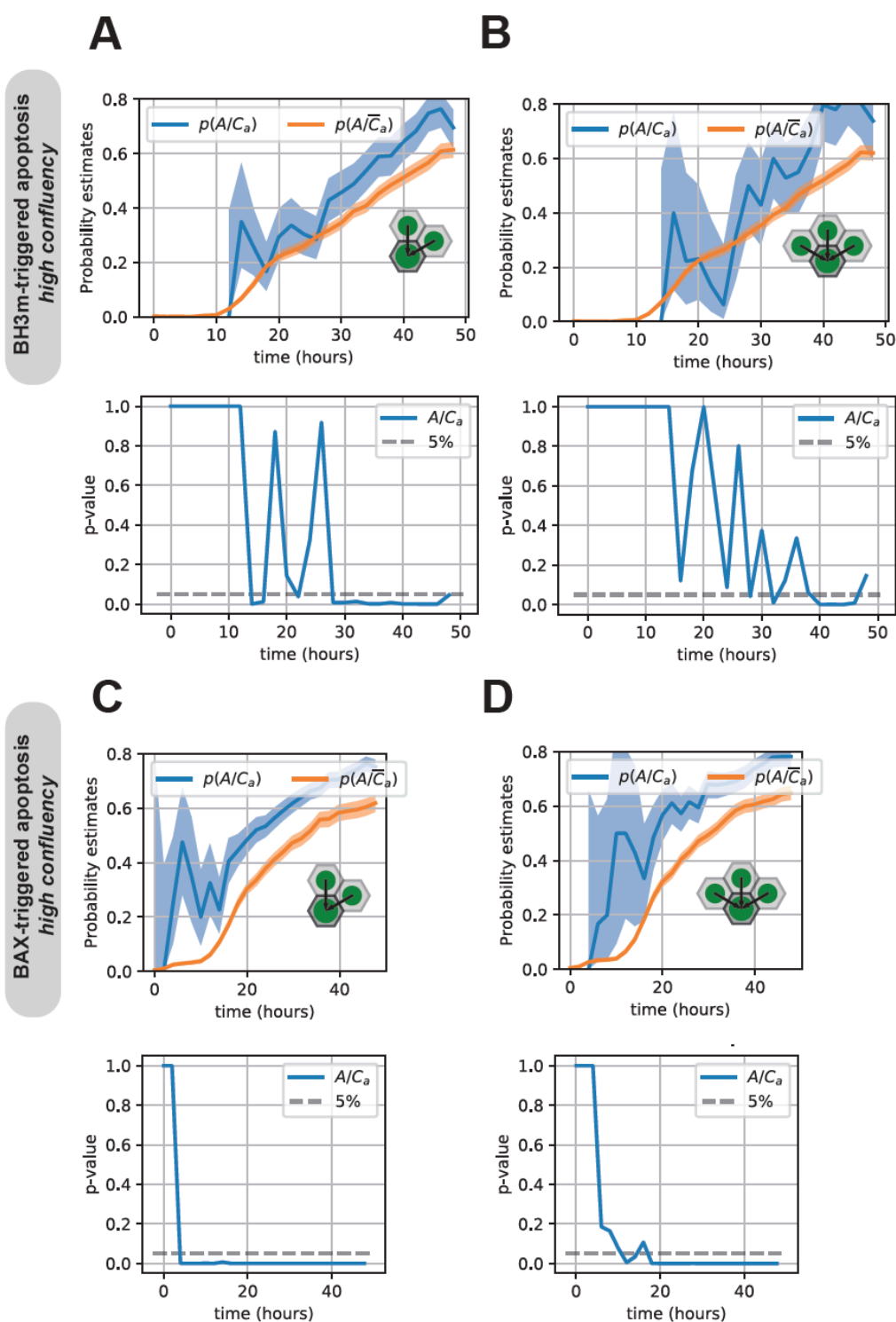
538

539

540

541

## Supplementary Figure 2



571

572

573

574

575

## 576 References

- 577 1. A. Strasser, D. L. Vaux, Cell Death in the Origin and Treatment of  
578 Cancer. *Molecular cell* **78**, 1045-1054 (2020).
- 579 2. B. A. Carneiro, W. S. El-Deiry, Targeting apoptosis in cancer therapy.  
580 *Nature reviews. Clinical oncology* **17**, 395-417 (2020).
- 581 3. L. S. Dickens, I. R. Powley, M. A. Hughes, M. MacFarlane, The  
582 'complexities' of life and death: death receptor signalling platforms. *Exp*  
583 *Cell Res* **318**, 1269-1277 (2012).
- 584 4. F. J. Bock, S. W. G. Tait, Mitochondria as multifaceted regulators of  
585 cell death. *Nature reviews. Molecular cell biology* **21**, 85-100 (2020).
- 586 5. G. Ichim, J. Lopez, S. U. Ahmed, N. Muthalagu, E. Giampazolias, M. E.  
587 Delgado, M. Haller, J. S. Riley, S. M. Mason, D. Athineos, M. J.  
588 Parsons, B. van de Kooij, L. Bouchier-Hayes, A. J. Chalmers, R. W.  
589 Rooswinkel, A. Oberst, K. Blyth, M. Rehm, D. J. Murphy, S. W. G. Tait,  
590 Limited mitochondrial permeabilization causes DNA damage and  
591 genomic instability in the absence of cell death. *Molecular cell* **57**, 860-  
592 872 (2015).
- 593 6. Y. N. Gong, C. Guy, H. Olauson, J. U. Becker, M. Yang, P. Fitzgerald,  
594 A. Linkermann, D. R. Green, ESCRT-III Acts Downstream of MLKL to  
595 Regulate Necroptotic Cell Death and Its Consequences. *Cell* **169**, 286-  
596 300 e216 (2017).
- 597 7. Y. N. Gong, J. C. Crawford, B. L. Heckmann, D. R. Green, To the edge  
598 of cell death and back. *FEBS J* **286**, 430-440 (2019).
- 599 8. A. L. Paek, J. C. Liu, A. Loewer, W. C. Forrester, G. Lahav, Cell-to-Cell  
600 Variation in p53 Dynamics Leads to Fractional Killing. *Cell* **165**, 631-  
601 642 (2016).
- 602 9. P. A. Gagliardi, M. Dobrzyński, M. A. Jacques, C. Dessauges, P.  
603 Ender, Y. Blum, R. M. Hughes, A. R. Cohen, O. Pertz, Collective  
604 ERK/Akt activity waves orchestrate epithelial homeostasis by driving  
605 apoptosis-induced survival. *Developmental cell* **56**, 1712-1726.e1716  
606 (2021).
- 607 10. F. J. Bock, C. Cloix, D. Zerbst, S. W. G. Tait, Apoptosis-induced FGF  
608 signalling promotes non-cell autonomous resistance to cell death.  
609 *bioRxiv*, 2020.2007.2012.199430 (2020).
- 610 11. R. Ankawa, N. Goldberger, Y. Yosefzon, E. Koren, M. Yusupova, D.  
611 Rosner, A. Feldman, S. Baror-Sebban, Y. Buganim, D. J. Simon, M.  
612 Tessier-Lavigne, Y. Fuchs, Apoptotic cells represent a dynamic stem  
613 cell niche governing proliferation and tissue regeneration.  
614 *Developmental cell*, (2021).
- 615 12. T. Kawaue, I. Yow, A. P. Le, Y. Lou, M. Loberas, M. Shagirov, J. Prost,  
616 T. Hiraiwa, B. Ladoux, Y. Toyama, Mechanics defines the spatial  
617 pattern of compensatory proliferation. *bioRxiv*, 2021.2007.2004.451019  
618 (2021).
- 619 13. M. R. Ruff, G. E. Gifford, Rabbit tumor necrosis factor: mechanism of  
620 action. *Infection and immunity* **31**, 380-385 (1981).
- 621 14. N. Reuven, J. Adler, V. Meltser, Y. Shaul, The Hippo pathway kinase  
622 Lats2 prevents DNA damage-induced apoptosis through inhibition of  
623 the tyrosine kinase c-Abl. *Cell death and differentiation* **20**, 1330-1340  
624 (2013).

- 625 15. J. Bar, E. Cohen-Noyman, B. Geiger, M. Oren, Attenuation of the p53  
626 response to DNA damage by high cell density. *Oncogene* **23**, 2128-  
627 2137 (2004).
- 628 16. Q. Ma, Y. Wang, A. S. Lo, E. M. Gomes, R. P. Junghans, Cell density  
629 plays a critical role in ex vivo expansion of T cells for adoptive  
630 immunotherapy. *Journal of biomedicine & biotechnology* **2010**, 386545  
631 (2010).
- 632 17. K. Kühn, S. Hashimoto, M. Lotz, Cell density modulates apoptosis in  
633 human articular chondrocytes. *Journal of cellular physiology* **180**, 439-  
634 447 (1999).
- 635 18. P. D. Bhola, S. M. Simon, Determinism and divergence of apoptosis  
636 susceptibility in mammalian cells. *Journal of cell science* **122**, 4296-  
637 4302 (2009).
- 638 19. S. L. Spencer, S. Gaudet, J. G. Albeck, J. M. Burke, P. K. Sorger, Non-  
639 genetic origins of cell-to-cell variability in TRAIL-induced apoptosis.  
640 *Nature* **459**, 428-432 (2009).
- 641 20. Y. Oren, M. Tsabar, M. S. Cuoco, L. Amir-Zilberstein, H. F. Cabanos, J.  
642 C. Hütter, B. Hu, P. I. Thakore, M. Tabaka, C. P. Fulco, W. Colgan, B.  
643 M. Cuevas, S. A. Hurvitz, D. J. Slamon, A. Deik, K. A. Pierce, C. Clish,  
644 A. N. Hata, E. Zaganjor, G. Lahav, K. Politi, J. S. Brugge, A. Regev,  
645 Cycling cancer persister cells arise from lineages with distinct  
646 programs. *Nature*, (2021).
- 647 21. G. C. Forcina, M. Conlon, A. Wells, J. Y. Cao, S. J. Dixon, Systematic  
648 Quantification of Population Cell Death Kinetics in Mammalian Cells.  
649 *Cell systems* **4**, 600-610.e606 (2017).
- 650 22. Z. Inde, G. C. Forcina, K. Denton, S. J. Dixon, Kinetic Heterogeneity of  
651 Cancer Cell Fractional Killing. *Cell reports* **32**, 107845 (2020).
- 652 23. A. Pérez-Garijo, Y. Fuchs, H. Steller, Apoptotic cells can induce non-  
653 autonomous apoptosis through the TNF pathway. *Elife* **2**, e01004  
654 (2013).
- 655 24. M. Riegman, M. S. Bradbury, M. Overholtzer, Population Dynamics in  
656 Cell Death: Mechanisms of Propagation. *Trends Cancer* **5**, 558-568  
657 (2019).
- 658 25. A. Linkermann, R. Skouta, N. Himmerkus, S. R. Mulay, C. Dewitz, F.  
659 De Zen, A. Prokai, G. Zuchriegel, F. Krombach, P. S. Welz, R.  
660 Weinlich, T. Vanden Berghe, P. Vandenabeele, M. Pasparakis, M.  
661 Bleich, J. M. Weinberg, C. A. Reichel, J. H. Bräsen, U. Kunzendorf, H.  
662 J. Anders, B. R. Stockwell, D. R. Green, S. Krautwald, Synchronized  
663 renal tubular cell death involves ferroptosis. *Proceedings of the  
664 National Academy of Sciences of the United States of America* **111**,  
665 16836-16841 (2014).
- 666 26. M. Riegman, L. Sagie, C. Galed, T. Levin, N. Steinberg, S. J. Dixon, U.  
667 Wiesner, M. S. Bradbury, P. Niethammer, A. Zaritsky, M. Overholtzer,  
668 Ferroptosis occurs through an osmotic mechanism and propagates  
669 independently of cell rupture. *Nature cell biology* **22**, 1042-1048 (2020).
- 670 27. F. Li, Q. Huang, J. Chen, Y. Peng, D. R. Roop, J. S. Bedford, C. Y. Li,  
671 Apoptotic cells activate the "phoenix rising" pathway to promote wound  
672 healing and tissue regeneration. *Science signaling* **3**, ra13 (2010).

- 673 28. E. Kowarz, D. Loscher, R. Marschalek, Optimized Sleeping Beauty  
674 transposons rapidly generate stable transgenic cell lines. *Biotechnol J*  
675 **10**, 647-653 (2015).  
676